The Astrophysical Journal, 749:46 (8pp), 2012 April 10 doi:10.1088/0004-637X/749/1/46

CARMA FOLLOW-UP OF THE NORTHERN UNCONFIRMED *PLANCK* GALAXY CLUSTER CANDIDATES

Stephen Muchovej[1,2], Erik Leitch[1,3], Thomas Culverhouse[1], John Carpenter[2], and Jonathan Sievers[4]
[1] California Institute of Technology, Owens Valley Radio Observatory, Big Pine, CA 93513, USA
[2] California Institute of Technology, Department of Astronomy, Pasadena, CA 91125, USA
[3] Department of Astronomy and Astrophysics, Kavli Institute for Cosmological Physics, University of Chicago, Chicago, IL 60637, USA
[4] CITA, University of Toronto, 60 St. George St., Toronto ON, M5S 3H8, Canada
Received 2011 December 4; accepted 2012 February 2; published 2012 March 20

ABSTRACT

We present the Combined Array for Research in Millimeter-wave Astronomy (CARMA) observations of the three northern unconfirmed galaxy clusters discovered by the *Planck* satellite. We confirm the existence of two massive clusters (PLCKESZ G115.71+17.52 and PLCKESZ G121.11+57.01) at high significance. For these clusters, we present refined centroid locations from the 31 GHz CARMA data, as well as mass estimates obtained from a joint analysis of CARMA and *Planck* data. We do not detect the third candidate, PLCKESZ G189.84−37.24, and place an upper limit on its mass of $M_{500} < 3.2 \times 10^{14}\ M_{\odot}$ at 68% confidence. Considering our data and the characteristics of the *Planck* Early Sunyaev–Zel'dovich (ESZ) Catalog, we conclude that this object is likely to be a cold-core object in the plane of our Galaxy. As a result, we estimate the purity of the ESZ Catalog to be greater than 99.5%.

Key words: galaxies: clusters: individual (PLCKESZ G115.71+17.52, PLCKESZ G121.11+57.01, PLCKESZ G189.84−37.24) – techniques: interferometric

Online-only material: color figure

1. INTRODUCTION

Galaxy clusters are the most massive, gravitationally bound structures in the universe. Over a Hubble time, they form from the rare, high-density peaks in the primordial density field on scales of ∼10 Mpc. As the abundance of galaxy clusters depends critically on the matter power spectrum and the expansion rate, cluster surveys are a sensitive probe of cosmological parameters such as the matter power spectrum normalization σ_8 and the dark energy equation of state w.

The Sunyaev–Zel'dovich (SZ) effect is a spectral distortion of the cosmic microwave background (CMB) radiation caused by inverse Compton scattering of the CMB photons by electrons in the hot intracluster medium (ICM; Sunyaev & Zel'dovich 1970, 1972; see also Birkinshaw 1999). The magnitude of the effect is proportional to the integrated pressure of the ICM, i.e., the density of electrons along the line of sight, weighted by the electron temperature. The integrated SZ flux of a cluster is therefore a measure of its total thermal energy.

The change in the observed brightness of the CMB caused by the SZ effect is given by

$$\frac{\Delta T_{\rm CMB}}{T_{\rm CMB}} = f(x) \int \sigma_{\rm T} n_e \frac{k_B T_e}{m_e c^2} dl \equiv f(x) y, \qquad (1)$$

where $T_{\rm CMB}$ is the cosmic microwave background temperature (2.73 K), $\sigma_{\rm T}$ is the Thomson scattering cross section, k_B is Boltzmann's constant, c is the speed of light, and m_e, n_e, and T_e are the electron mass, number density and temperature. Equation (1) defines the Compton y-parameter. The frequency dependence of the SZ effect is contained in the term

$$f(x) = \left(x \frac{e^x + 1}{e^x - 1} - 4 \right) (1 + \delta_{\rm SZ}(x, T_e)), \qquad (2)$$

where $x \equiv h\nu / k_B T_{\rm CMB}$, h is Planck's constant, and $\delta_{\rm SZ}$ is a relativistic correction, for which we adopt the Itoh et al. (1998) calculation, valid to fifth order in $k_B T_e / m_e c^2$. The SZ effect appears as a temperature decrement at frequencies below ≈218 GHz, and an increment at higher frequencies.

The redshift independence of the SZ effect in both brightness and frequency (the ratio $\Delta T / T$ in Equation (1) is independent of the distance to the cluster) offers enormous potential for finding high-redshift clusters. Searches for massive galaxy clusters via the SZ effect have the potential to produce cluster catalogs with a simple mass selection, nearly independent of redshift if the angular resolution of the observations is sufficient to resolve the cluster (Carlstrom et al. 2002). As a result, several experiments have recently conducted searches for galaxy clusters via their SZ effect, e.g., the Sunyaev–Zel'dovich Array (SZA; Muchovej et al. 2011)—now a part of the Combined Array for Research in Millimeter-wave Astronomy (CARMA), the South Pole Telescope (SPT; Vanderlinde et al. 2010), the Arcminute Microkelvin Imager (AMI; Jones 2002), and the Atacama Cosmology Telescope (ACT; Marriage et al. 2011). Most recently, the *Planck* space telescope has begun to measure the CMB over the whole sky in nine bands, and at lower resolution (∼5′), to search for massive clusters of galaxies via their SZ effect (Planck Collaboration et al. 2011a).

The *Planck* Early Release Compact Source Catalogue has identified 189 clusters of galaxies, including 20 previously unknown clusters. Of these, 11 have been confirmed using *XMM-Newton*, and 1 was confirmed using a combination of AMI and *WISE* data (Planck Collaboration et al. 2011a). As a result, eight objects from the catalog were unconfirmed at the time of the *Planck* early release, and over the past year various groups in the astronomical community have sought to confirm their existence and infer properties about these newly discovered objects. In particular, the SPT was used to confirm all cluster candidates in the southern sky and AMI targeted the two northernmost clusters, confirming one of them in conjunction with *WISE* (Story et al. 2011; AMI Consortium et al. 2011; Wen et al. 2009). In this paper, we present SZ follow-up observations obtained with CARMA of the three clusters visible from the northern sky: PLCKESZ G115.71+17.52, PLCKESZ G121.11+57.01, and PLCKESZ G189.84−37.24.

Whereas the *Planck* data are sensitive to the bulk SZ signal (resolution of ∼5′), measuring the pressure profile of these clusters requires SZ follow-up with higher-resolution instruments.

Table 1
Cluster Observations

Cluster Name	Pointing Center (J2000)		t_{int}[a]	Short Baselines (0–2kλ)		Long Baselines (2–8kλ)	
	α	δ	(hr)	Beam($'' \times ''\angle$)[b]	σ(mJy)[c]	Beam($'' \times ''\angle$)[b]	σ(mJy)[c]
PLCKESZ G115.71+17.52	$22^h26^m24^s.89$	$78°18'16''.11$	9.3	118.2×146.5 −34.5	0.41	12.7×19.9 39.7	0.41
PLCKESZ G121.11+57.01	$12^h59^m23^s.77$	$60°05'24''.64$	8.0	138.8×146.0 −52.8	0.47	15.9×19.8 43.3	0.50
PLCKESZ G189.84−37.24	$03^h59^m45^s.80$	$00°06'41''.75$	5.8	105.2×112.7 36.9	0.43	15.7×23.2 37.1	0.51

Notes.
[a] On-source integration time, unflagged data.
[b] Synthesized beam FWHM and position angle measured from north through east.
[c] Achieved rms noise in corresponding maps.

As we demonstrate in this work, the combination of the two data sets yields an improved estimate of the cluster mass, which is of particular interest to the calibration of SZ observables to intrinsic cluster parameters. This paper is organized as follows: we present a description of the data and the resulting maps in Section 2, and derived cluster properties in Sections 3 and 4. We present a discussion and conclusion in Sections 5 and 6, respectively.

2. CARMA OBSERVATIONS

2.1. Observations and Reduction

The data presented in this paper were collected in ten separate observations with the compact 31 GHz sub-array of CARMA. This compact sub-array, formerly known as the SZA, consists of eight 3.5 m telescopes operating from 27–35 GHz, arranged such that six of the telescopes are in a compact configuration with two outlying telescopes to allow identification and removal of compact sources. Data from the six-element compact array are referred to as *short-baseline* data below, while the data from the two outlying telescopes are referred to as *long-baseline* data. The array layout is similar to that presented in Muchovej et al. (2007), with the main difference being that one of the long east–west baselines has been changed to a north–south baseline.

Over the time period from 2011 June to 2011 August, each cluster was observed for 4–5 hr about transit, in an array configuration designed to minimize shadowing by other antennas in the array principally for sources at low declinations. We require that clusters are observed at an elevation greater than 30 deg (to minimize atmospheric contamination) for at least two hours during the day. This limited our observations to the three unconfirmed *Planck* clusters in the northern hemisphere. Cluster observations were interleaved with observations of a strong unresolved source every 15 minutes to monitor variations in the instrumental gain. PLCKESZ G115.71+17.52 was observed over four tracks for a total of 9.3 hr of unflagged on-source data. Likewise, we obtained 8.0 hr of unflagged on-source data over three tracks on PLCKESZ G121.11+57.01, and 5.8 hr of unflagged data on PLCKESZ G189.84−37.24 obtained over three tracks. Data were converted from the MIRIAD format to Matlab, and calibrated in the same pipeline outlined in Muchovej et al. (2007). Absolute calibration is derived from observations of Mars, using fluxes predicted by the most up-to-date Rudy model scaled by 2% to match the latest *Wilkinson Microwave Anisotropy Probe* (*WMAP*) measurements (Rudy 1987; Weiland et al. 2011). We estimate the flux calibration to be good to 5% via long-time monitoring of flux calibrators used by the SZA. In Table 1, we give the pointing center of the cluster along with details of the observations, including the synthesized beam sizes for both the short- and long-baseline data. We also present the achieved rms flux sensitivities for maps made with short- and long-baseline data. The effect of the array being in an orientation optimized for low-declination sources is evident upon inspection of the sensitivities achieved for each of the fields. In particular, a greater number of inner-array antennas are shadowed when observing sources at higher declination. As a result, observations of sources at high declination can require a longer integration time to achieve the same rms sensitivity as observations of low-declination sources.

2.2. Resulting Maps

In the limit where sky curvature is negligible over the instrument's field of view, the response of an interferometer on a single baseline, known as a *visibility*, can be approximated by

$$V(u,v) = \int\int_{-\infty}^{+\infty} A_N(l,m) I(l,m) \times \exp\{-2\pi j[ul+vm]\} dl\, dm, \quad (3)$$

where u and v are the baseline lengths projected onto the sky, l and m are direction cosines measured with respect to the (u, v) axes, $A_N(l, m)$ is the normalized antenna beam pattern, and $I(l,m)$ is the sky intensity distribution.

As implied by Equation (3), an image of the source intensity multiplied by the antenna beam pattern, also known as a *dirty map*, can be recovered by Fourier transform of the visibility data. Note that in addition to modulation by the primary beam, structure in the dirty map is convolved with a function that reflects the incomplete Fourier-space sampling of a given observation. This filter function is the *synthesized beam*, equivalent to the point-spread function for the interferometer. A *clean* map is an image from which the synthesized beam pattern has been deconvolved, and the source model reconvolved with a Gaussian fit to the central lobe of the synthesized beam.

In the first column of Figure 1, we present the aggregate u–v coverage for observations of PLCKESZ G115.71+17.52, PLCKESZ G121.11+57.01, and PLCKESZ G189.84−37.24. The second and third columns depict the corresponding *dirty* maps obtained from the long- and short-baseline data, respectively. We identify two sources of emission in the field of PLCKESZ G115.71+17.52, corresponding to known sources from the NVSS catalog. As no NVSS or FIRST coverage is available for the PLCKESZ G121.11+57.01 and PLCKESZ G189.84−37.24 fields, we use the combination of the short- and long-baseline data to identify sources of emission directly from the SZA data at greater than 3.5 times the map rms level. We identify one compact source in the field of PLCKESZ G121.11+57.01 at four times the map rms. We do not identify any sources of emission at a significance greater than

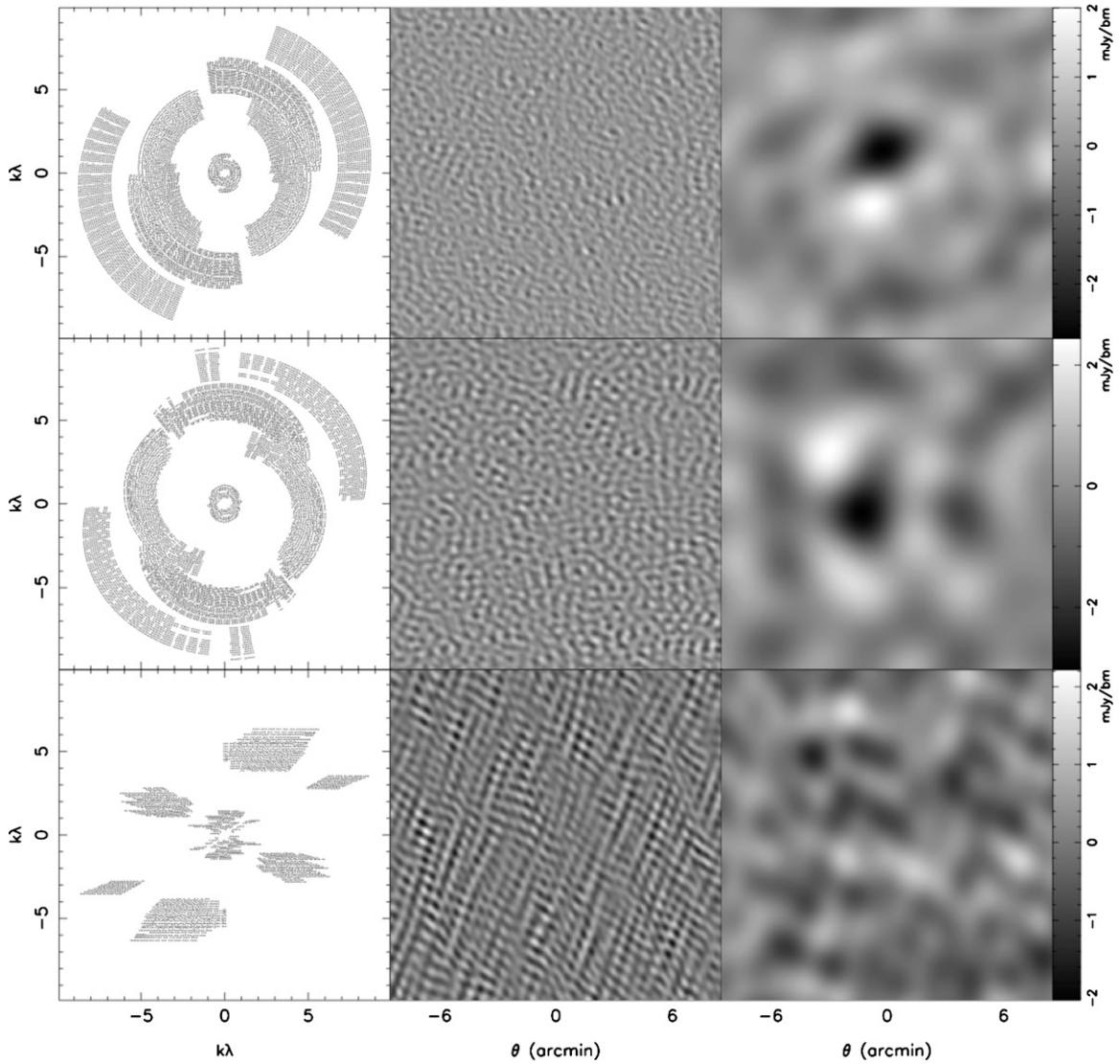

Figure 1. Tow Row: u–v coverage, long-baseline dirty map, and short-baseline dirty map of data collected toward PLCKESZ G115.71+17.52. Middle Row: corresponding plots for field of PLCKESZ G121.11+57.01. Bottom Row: same, but for PLCKESZ G189.84−37.24. Sensitivity and resolutions of observations are presented in Table 1.

Table 2
Unresolved Radio Sources

Cluster Field	No.	R.A. (J2000)	$\sigma_{\rm R.A.}$ (s)	Decl. (J2000)	$\sigma_{\rm Decl.}$ ($''$)	d[a] ($'$)	31 GHz Flux (mJy)	1.4 GHz flux[b] (mJy)	α (1.4/31 GHz)
PLCKESZ G115.71+17.52	1	$22^{\rm h}26^{\rm m}49\overset{\rm s}{.}19$	0.20	$+78^\circ16'53\overset{''}{.}8$	3.1	1.84	0.97 ± 0.25	30.88 ± 1.66	1.11 ± 0.08
	2	$22^{\rm h}26^{\rm m}36\overset{\rm s}{.}44$	... [c]	$+78^\circ15'25\overset{''}{.}9$	... [c]	2.90	0.47 ± 0.21	3.68 ± 0.55	0.71 ± 0.20
PLCKESZ G121.11+57.01	1	$12^{\rm h}59^{\rm m}46\overset{\rm s}{.}06$	0.27	$+60^\circ07'09\overset{''}{.}8$	3.5	3.28	1.76 ± 0.43		

Notes.
[a] Distance from observation pointing center.
[b] Integrated NVSS flux at 1.4 GHz.
[c] Due to low signal-to-noise ratio, location fixed to NVSS centroid.

3.5 times the map rms level in the field toward PLCKESZ G189.84−37.24. The location and fluxes of these sources are presented in Table 2. We note that the sparseness of our Fourier sampling of PLCKESZ G189.84−37.24 does not hinder our ability to detect sources of emission, as we are sensitive to scales as large as $4\overset{'}{.}5$. The main effect of the sparse sampling is on the shape of the *synthesized beam*, not our ability to detect extended sources of emission.

As seen in the last column in Figure 1, we detect an SZ decrement toward PLCKESZ G115.71+17.52 and PLCKESZ G121.11+57.01 at 6.1 and 6.0 times the rms noise values in the map, respectively. We detect no decrement toward PLCKESZ G189.84−37.24. We note that the images shown in Figure 1 are for display purposes only, and that all source and cluster fluxes are fit directly in the Fourier plane, as described in Section 3.

3. CLUSTER PARAMETER ESTIMATION

All quantitative results presented in this paper are derived from simultaneously fit models of the SZ cluster decrement and contaminating sources, as detailed below. In all cases, the model is constructed in the image plane, multiplied by the primary beam, and Fourier transformed, as indicated in Equation (3). The resulting model visibilities are compared directly to the calibrated visibility data. In this way all fitting is done in the Fourier-plane, where the visibility noise covariance is diagonal and the spatial filtering of the interferometer is trivial to implement; maps are used only for examination of the data and to identify cases where contaminating sources are present.

The frequency-dependent shape of the primary beam used in the analysis is calculated from the Fourier transform of the aperture illumination of the telescopes, modeled as a Gaussian taper with a central obscuration corresponding to the secondary mirror. The validity of this model has been confirmed by holographic measurements.

We fit unresolved radio sources, hereafter referred to as *point sources*, as delta functions, parameterized by the intensity at the band center, $I_{31\,\mathrm{GHz}}$, and a spectral index α over our 16 500 MHz wide correlator bands. The point source intensity at frequency ν is then:

$$I_{ps}(l,m) = I_{31\,\mathrm{GHz}}\left(\frac{\nu}{31\,\mathrm{GHz}}\right)^{-\alpha}\delta(l-l')\,\delta(m-m'), \quad (4)$$

where l' and m' are the coordinates of the point source on the sky. From Equations (3) and (4), it can be seen that the visibility amplitude due to a point source is simply its intensity, weighted by the normalized primary beam response at the source location.

We model the cluster gas density by a spherical, isothermal β-model, described by

$$n_e(r) = n_{e0}\left(1+\frac{r^2}{r_c^2}\right)^{-3\beta/2}, \quad (5)$$

where the core radius r_c and the power-law index β are shape parameters, and n_{e0} is the central electron number density. The model is a simple parameterization of the gas density profile traditionally used in fitting X-ray (cf. Mohr et al. 1999) and SZ data. Although more complex parameterizations can be shown to better reproduce fine details of the density and temperature profiles of simulated clusters, when applied to realistic data with the resolution of the SZA in this configuration, the differences are irrelevant. As a result, gas-mass and total-mass estimates derived from the isothermal β-model diverge from results obtained with more sophisticated pressure profiles only at the cluster outskirts, and have been demonstrated to be consistent with each other intermediate cluster radii (see Table 5 in Mroczkowski et al. 2009).

The corresponding SZ temperature decrement is given by

$$\Delta T\,(\theta) = \Delta T_0\left(1+\frac{\theta^2}{\theta_c^2}\right)^{\frac{1}{2}-\frac{3\beta}{2}}, \quad (6)$$

where $\theta = r/D_A$, $\theta_c = r_c/D_A$, and D_A is the angular diameter distance. Under the assumption that the gas is isothermal, the temperature decrement at zero projected radius, ΔT_0, is related to n_{e0} by

$$n_{e0} = \frac{\Delta T_0}{T_{CMB}}\frac{m_e c^2}{f(x)k_B\sigma_T}\frac{1}{T_e}\frac{1}{\sqrt{\pi}\,D_A\theta_c}\frac{\Gamma\left(\frac{3\beta}{2}\right)}{\Gamma\left(\frac{3\beta}{2}-\frac{1}{2}\right)}. \quad (7)$$

Table 3
CARMA Centroid Offsets from *Planck*

Cluster Name	ΔR.A. (″)	ΔDecl. (″)
PLCKESZ G115.71+17.52	$22.3^{+6.3}_{-12.7}$	$70.4^{+11.1}_{-6.9}$
PLCKESZ G121.11+57.01	$84.5^{+18.0}_{-11.0}$	$-15.1^{+10.1}_{-15.1}$

Best-fit values for the model parameters are determined using a Monte Carlo Markov Chain analysis (MCMC; Bonamente et al. 2004, 2006; LaRoque et al. 2006, and references therein). The Markov chains are a sampling of the multi-dimensional likelihood for the model parameters, given the SZ data; the histogram of values in the chain for each parameter is thus an estimate of the probability distribution for that parameter, marginalized over the other model parameters. The parameter β was fixed to 0.86, consistent with the average shape of massive clusters determined from the analysis of 15 massive clusters with SPT (Plagge et al. 2010). This represents a shift from previous joint analyses of X-ray and SZ observations which traditionally used β values of 2/3 (e.g., Mohr et al. 1999; LaRoque et al. 2006).

In Table 3, we present offsets from the *Planck* centroids determined for PLCKESZ G115.71+17.52 and PLCKESZ G121.11+57.01. For these and all other quantities determined from the Markov chains, we quote the maximum-likelihood value, with an uncertainty obtained by integrating the distribution for that quantity to a fixed probability density, until 68% of the probability is enclosed.

4. SZ TEMPERATURE AND MASS ESTIMATES

In this section, we describe how the cluster electron temperature, gas mass and total mass are determined from the Markov chains of model parameters described in Section 3.

An estimate of the gas mass in the cluster can be obtained by multiplying Equation (5) by $\mu_e m_p$, the mean mass per electron of the ions in the plasma, and integrating the result to the desired radius:

$$M_{\mathrm{gas}}(R) = \mu_e m_p n_{e0}\int_0^R\left(1+\frac{r^2}{r_c^2}\right)^{-3\beta/2}4\pi r^2 dr. \quad (8)$$

The central electron density n_{e0} is a function of the electron temperature T_e (assumed to be constant) and the model parameters ΔT_0, β and θ_c, as given by Equation (7).

The total mass of the cluster can be estimated by assuming hydrostatic equilibrium (hereafter HSE) and only thermal pressure support (i.e., no turbulent or rotational support). For the electron distribution given by Equation (5), this approximation yields an analytic solution for the total cluster mass contained within a radius R of

$$M_{\mathrm{total}}(R) = \frac{3k_B T_e\beta}{G\mu m_p}\frac{R^3}{r_c^2+R^2}, \quad (9)$$

where G is the gravitational constant, μm_p is the mean molecular mass of the gas, and r_c is the core radius, related to θ_c by the angular diameter distance. We adopt a value of 0.3 $Z_\odot$ for the cluster metallicity when calculating both μ_e and μ, and assume a ΛCDM cosmology with parameters fixed to those from the *WMAP* seven-year analysis in all subsequent calculations (Larson et al. 2011).

From Equations (7)–(9), we see that if we assume a value for the ratio of the gas mass to the total cluster mass, hereafter referred to as the *gas-mass fraction*, f_{gas}, an estimate of

Table 4
Cluster Masses and ICM Properties Derived from SZ Data

Cluster Name	Prior		Quantities within $R_{2500(z)}$		Quantities within $R_{500(z)}$	
		T_e (keV)	$M_{\rm gas}$ ($10^{12}\,M_\odot$)	$M_{\rm total}$ ($10^{13}\,M_\odot$)	$M_{\rm gas}$ ($10^{12}\,M_\odot$)	$M_{\rm total}$ ($10^{13}\,M_\odot$)
PLCKESZ G115.71+17.52	None	$5.3^{+1.1+0.2}_{-0.9-0.2}$	$29.2^{+4.6+2.3}_{-4.6-2.6}$	$24.0^{+6.7+1.1}_{-5.4-3.2}$	$51.9^{+12.0+1.5}_{-9.0-1.2}$	$53.7^{+18.0+5.9}_{-12.0-6.2}$
PLCKESZ G115.71+17.52	*Planck*[a]	$4.9^{+1.0+0.2}_{-0.6-0.2}$	$28.8^{+4.9+2.3}_{-4.9-2.6}$	$21.6^{+8.1+1.1}_{-3.4-3.2}$	$51.8^{+11.2+1.5}_{-11.2-1.2}$	$51.5^{+15.8+5.9}_{-10.5-6.2}$
PLCKESZ G121.11+57.01	None	$6.4^{+1.5+0.2}_{-1.5-0.2}$	$24.6^{+5.8+2.3}_{-8.2-0.9}$	$15.9^{+10.5+3.2}_{-3.9-2.5}$	$81.0^{+15.0+2.1}_{-20.6-2.1}$	$61.5^{+26.6+9.4}_{-11.8-7.2}$
PLCKESZ G121.11+57.01	*Planck*[b]	$5.7^{+1.1+0.2}_{-1.1-0.2}$	$24.8^{+5.4+2.3}_{-7.7-0.9}$	$18.5^{+5.7+3.2}_{-6.6-2.5}$	$74.4^{+19.3+2.1}_{-19.3-2.1}$	$58.1^{+18.0+9.4}_{-11.9-7.2}$

Notes.
[a] $\theta = 14\farcm47$, $\sigma_\theta = 7.333$ from ESZ catalog.
[b] $\theta = 17\farcm99$, $\sigma_\theta = 5.902$ from ESZ catalog.

electron temperature can be inferred, allowing the masses to be determined without reference to an a priori value for T_e (cf. Joy et al. 2001; LaRoque et al. 2003). We employ this method below to obtain cluster properties from the SZ data. For comparison, spectroscopically determined electron temperatures from X-ray measurements can be used to estimate the gas masses, total masses, and $f_{\rm gas}$ directly from the Markov chains. A previous study of a sample of 38 massive clusters obtained a mean of $f_{\rm gas} = 0.116 \pm 0.005$, from masses evaluated within a radius of R_{2500} (LaRoque et al. 2006). In the calculation of the gas temperature for a single cluster, we therefore adopt a Gaussian distribution of $f_{\rm gas}$ with a mean of 0.116 and standard deviation of 0.030, where we have scaled the reported error in the mean by $\sqrt{37}$ to approximate the measured distribution of gas-mass fractions.

Calculating the gas mass by integrating Equation (8) requires knowledge of the redshift of the cluster (to determine the physical radius over which to integrate). As no redshift information is available for these objects, we marginalize over the redshift distribution of the newly discovered *Planck* clusters. This distribution consists of 17 objects whose redshifts are determined via either X-ray or optical follow-up, with a median redshift value of 0.32 (Planck Collaboration et al. 2011c; Story et al. 2011; Planck Collaboration et al. 2011a).

We calculate the masses from the Markov chains by sampling the distributions of θ_c, ΔT_0, $f_{\rm gas}$ and z, and solving for T_e at an overdensity radius of R_{2500} (where the estimates of $f_{\rm gas}$ are determined). The resulting best-estimates for the electron temperature are presented in Table 4. Equipped with estimates of the electron temperature, we can readily obtain estimates of the gas-mass and total cluster mass from Equations (8) and (9). In Table 4 we present these values for PLCKESZ G115.71+17.52 and PLCKESZ G121.11+57.01, integrated to an overdensity radius of R_{2500}, and to R_{500}, assuming that $f_{\rm gas}$ is constant with radius. The overdensity radius R_Δ is defined as the radius at which the mean density of the cluster is related to the critical density of the universe by a fixed density contrast $\Delta(z)$, where the density contrast is assumed to scale with redshift like the mean density of a virialized system, as determined from numerical simulations (Bryan & Norman 1998).

An interferometer has no ability to constrain the size of an object larger than the spatial scale of its shortest baselines. For CARMA at 31 GHz, the instrument is insensitive to scales $\gtrsim 10'$ on the sky. The *Planck* satellite, on the other hand, cannot constrain cluster models more compact than its highest resolution element (namely $5'$), but can readily constrain the size of larger objects. As a result, we obtain the tightest constraints on the cluster temperature and masses by including prior information on the angular size of these clusters from the *Planck* satellite. The *Planck* ESZ catalog presents a angular extent from these clusters (at $5\theta_{500}$) with an associated uncertainty. The resulting masses and temperatures, when this prior is included in the Markov chains, are also shown in Table 4. We see that including the *Planck* prior reduces the statistical uncertainty in our determinations of gas temperatures by 25%, and our final estimate of total masses by 15%–30%.

The choice of β is one of the dominant systematic uncertainties associated with our calculation. This effect is more pronounced on the cluster outskirts, where recent studies of the average cluster profile have shown an increasing power-law slope at higher radii (Arnaud et al. 2010; Sun et al. 2011). Plagge et al. (2010) determined a mean value of β of 0.86 ± 0.09 from the stacking analysis of 15 clusters. To estimate the error introduced by our choice of β, we repeat our analysis using values of 0.77 and 0.95. We see from Table 4 that this effect is largely negligible at the inner radii of clusters, and leads to a roughly 10% uncertainty at larger radii. We note that this uncertainty is still much smaller than the statistical uncertainty in our mass estimate.

5. DISCUSSION

5.1. PLCKESZ G115.71+17.52

We confirm the presence of a massive galaxy cluster corresponding to PLCKESZ G115.71+17.52. We determine the centroid of this cluster to be offset from the *Planck* location by slightly more than an arcminute, at R.A. 22:26:31.3, decl. +78:19:28.7. In the first two columns of Figure 2 we present the long- and short-baseline *dirty maps* of this cluster once sources of emission are removed. In the last column of the first row, we present the resulting cleaned image of this cluster. We estimate the mass of this cluster to be $M_{500} = 5.2^{+1.6+0.6}_{-1.1-0.6} \times 10^{14}\,M_\odot$, where the first set of errors corresponds to the 1σ statistical errors and the second set to the systematic uncertainty due to our choice of β (presented in Table 4). This value is consistent with the median mass of clusters released in the *Planck* ESZ catalog (Planck Collaboration et al. 2011a). We note that the inclusion of the *Planck* prior in our analysis improves our mass estimate by 15%, comparable to the error associated with our choice of β. As discussed in Section 4, the mass estimate was obtained assuming the redshift distribution of the newly discovered *Planck* clusters. As the SZ observations provide no information on the redshift of the cluster, we present our determination of the mass of this cluster as a function of redshift in Figure 3. We note that our final mass estimate for this cluster is consistent with that of the median redshift of the newly discovered *Planck* clusters, namely 0.32.

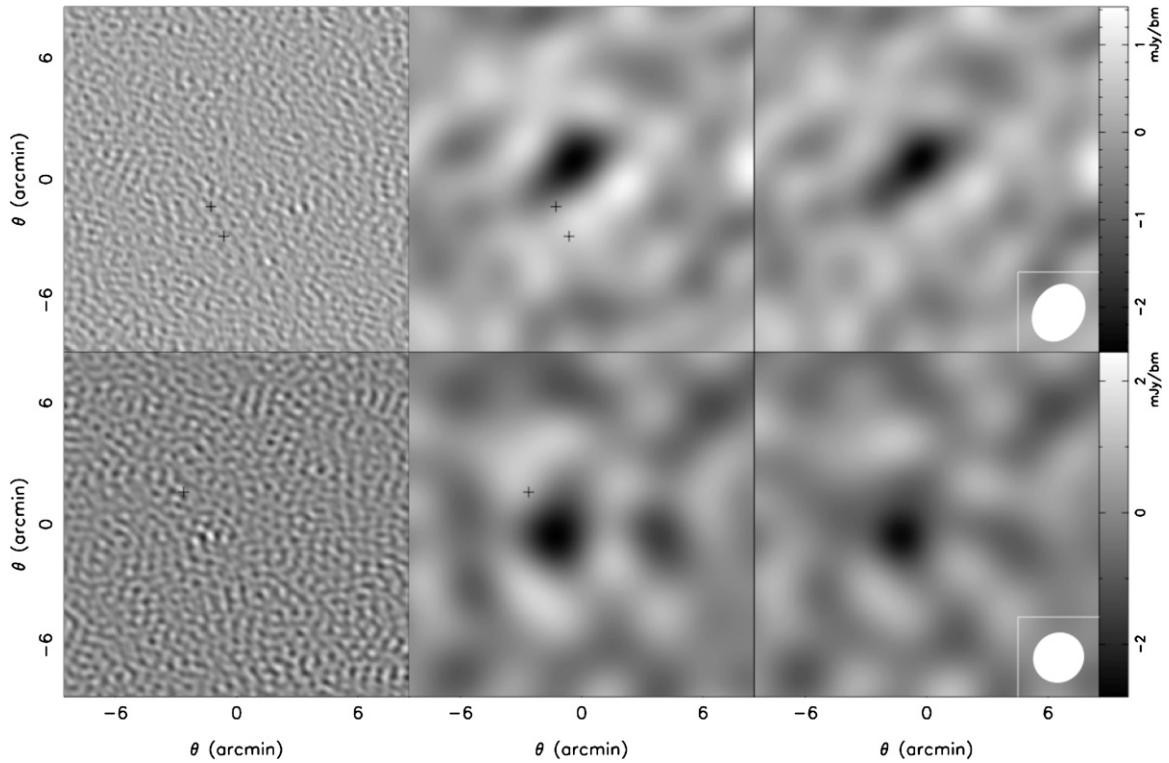

Figure 2. Top Row: PLCKESZ G115.71+17.52: long-baseline residual map once sources of emission are removed from the data; short-baseline residual map once sources are removed; cleaned map of PLCKESZ G115.71+17.52. Bottom Row: corresponding images for PLCKESZ G121.11+57.01. Locations of sources removed from the data are depicted by crosses.

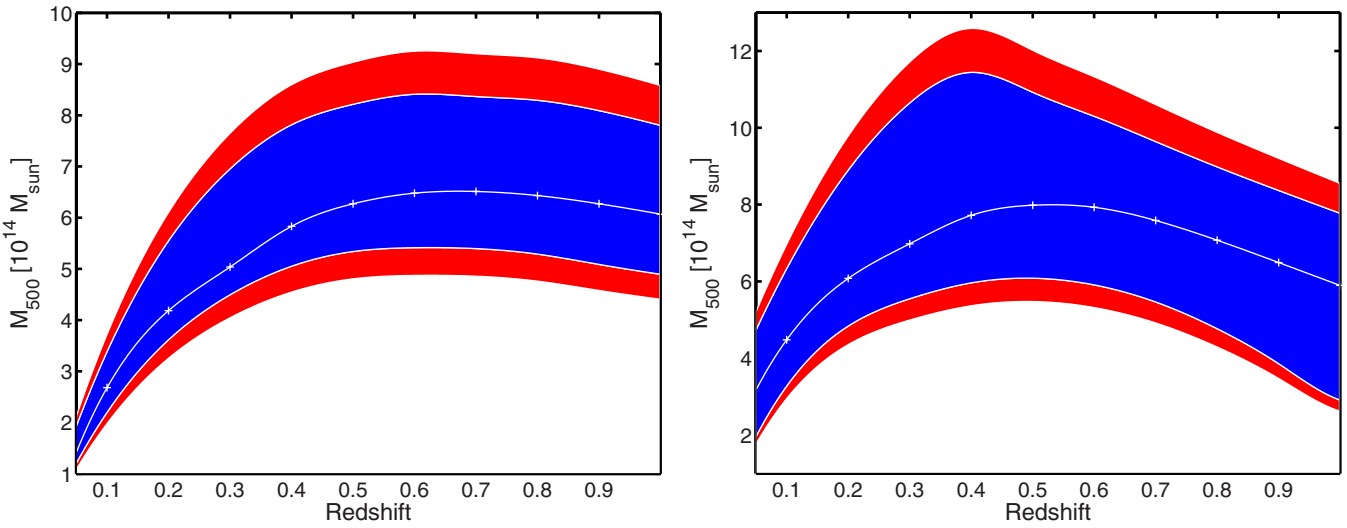

Figure 3. Left: mass estimate of PLCKESZ G115.71+17.52 as a function of redshift. The blue shaded region indicates the 1σ errors on the most likely value of the mass (center line), and the red shaded region is an estimate of the error due to the choice of β. Right: same plot, but for PLCKESZ G121.11+57.01. We note that our final mass estimates are consistent with the clusters being at a redshift $\sim$0.32, the median redshift value of the newly discovered *Planck* clusters.

(A color version of this figure is available in the online journal.)

We note that this field has also been observed with AMI; however, in the presence of overwhelming source contamination at 15 GHz, AMI was unable to detect an SZ decrement (AMI Consortium et al. 2011) and confirm this cluster. The CARMA data thus provide the first confirmation of this newly discovered cluster.

5.2. PLCKESZ G121.11+57.01

We detect a significant SZ decrement toward PLCKESZ G121.11+57.01, confirming its existence as a massive cluster. We estimate the mass of this cluster to be $M_{500} = 5.8^{+1.8+0.9}_{-1.2-0.7} \times 10^{14}\ M_{\odot}$, and find its centroid to be at R.A. 12:59:35.8, decl. +60:05:09.1. The inclusion of the *Planck* prior on the angular extent of this cluster reduces the uncertainty on our mass estimate by $\sim$28%. The cleaned image of this cluster, with a single source of emission removed from the field, can be found in the last panel of the second row in Figure 2. As no redshift information is available for this cluster, in the right panel of Figure 3 we present the estimated mass of this cluster as a function of redshift.

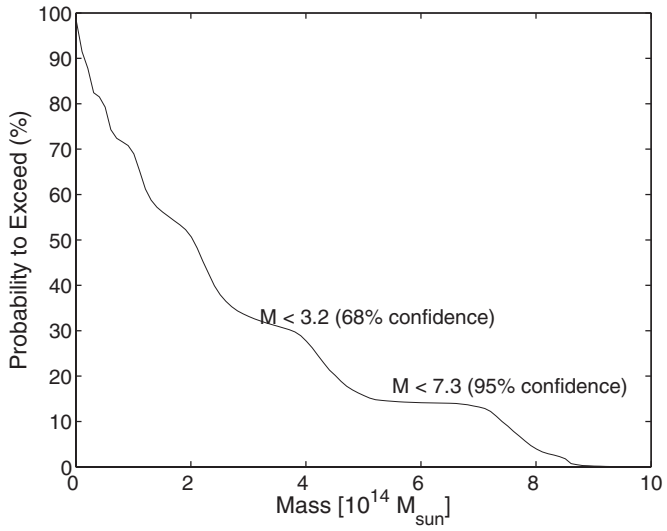

Figure 4. Mass limit (M_{500}) on PLCKESZ G189.84−37.24 obtained assuming a compact cluster within 1′ of the location indicated by the *Planck* ESZ catalog.

This cluster was previously confirmed with a 107 hr observation with AMI (AMI Consortium et al. 2011). We note that the cluster is detected with comparable significance in the 8 hr CARMA track, and that the determination of the cluster centroid agrees with that determined from AMI to 22″ (by comparison, the quoted accuracy on the AMI centroid is 20″).

5.3. PLCKESZ G189.84−37.24

We detect no SZ decrement at the location of PLCKESZ G189.84−37.24. Furthermore, as can be seen in Figure 1, the field is free of source contamination. A non-detection of a genuine cluster in a 6 hr track with CARMA would require either a low-mass compact cluster (SZ signal weak), or an extended, low-redshift cluster (SZ signal resolved out).

Under the assumption that a cluster is present within a one-arcminute radius of the *Planck* coordinate, and that it subtends the typical scales of clusters, we can place an upper limit on the mass of the cluster, given our data. A Markov chain is run as described in Section 3, and the formalism of Section 4 is applied to determine the distribution of masses allowed by our data. Under these assumptions, we can place an upper limit on the cluster mass (M_{500}) of $3.2{+}0.3 \times 10^{14}\ M_{\odot}$ at 68% confidence, where the uncertainty is due to the choice of β, as seen in Figure 4.

We note however that the *Planck* data indicate a size of 62.′5 at $5\theta_{500}$. An object this large would be undetectable (resolved out) by the interferometer, so it is not surprising that the CARMA data are consistent with noise, whatever the nature of the source seen by *Planck*. If this is a cluster, however, its angular extent indicates that it is nearby ($z \ll 0.1$), and the Y_{500} estimated from the *Planck* data implies an X-ray luminosity several times larger than either PLCKESZ G115.71+17.52 or PLCKESZ G121.11+57.01 (Melin et al. 2011; Planck Collaboration et al. 2011d), a source easily detectable with *ROSAT*. Yet the measured signal in RASS toward this object, integrated over the *Planck* aperture, is consistent with noise, and a factor of three to six lower than toward the compact clusters PLCKESZ G115.71+17.52 and PLCKESZ G121.11+57.01 (Planck Collaboration et al. 2011a). The interpretation of this source as a nearby cluster would therefore require unusual conditions in the ICM to produce little or no central condensation, leading to the selective suppression of X-rays relative to the SZ signal. Inspection of images from the Sloan Digital Sky Survey also reveal no evidence for an over-abundance of galaxies consistent with nearby clusters.

As a result, we believe that the most natural explanation for this source is the contamination discussed in Planck Collaboration et al. (2011a), where it is noted that the prevalence of IR sources emitting above 217 GHz, dust emission, and cold cores was found to be higher than expected. *Planck* identified many cool core objects near the Galactic plane, including a southern region around Galactic longitude of 180 extending south to longitude of −45° (Planck Collaboration et al. 2011b), in which this object lies. The inclusion of data from the low-frequency instrument (where the SZ signal, characterized by a decrement, can be readily distinguished from a thermal spectrum) in the *Planck* cluster-finding algorithm will clarify the nature of this source.

6. CONCLUSION

Of the new cluster candidates identified in the *Planck* Early Release Compact Source Catalogue, three are visible in the northern sky: PLCKESZ G115.71+17.52, PLCKESZ G121.11+57.01, and PLCKESZ G189.84−37.24. From 2011 June to August, we obtained 31 GHz observations of these candidates with the CARMA interferometer, with a total of 5–10 hr of observation per source.

SZ decrements are detected with high significance toward both PLCKESZ G115.71+17.52 and PLCKESZ G121.11+57.01; we present refined centroid locations and mass estimates at R_{2500} and R_{500} for each of these clusters. Masses are determined from the SZ data via an MCMC analysis, by assuming a distribution for the gas-mass fraction from previous studies of massive clusters, and by marginalizing over the redshift distribution of the newly discovered *Planck* clusters. These masses represent the first joint-analysis of Planck and interferometric SZ data. Masses were determined using the Planck priors on the size of the clusters, resulting in mass uncertainties of roughly 20%. An extension of this work to a larger sample of clusters already observed with CARMA will help tighten our constraints on SZ-scaling relations. These data represent the first confirmation of PLCKESZ G115.71+17.52, and the first mass estimate for either cluster.

No SZ decrement was detected in the CARMA observations toward PLCKESZ G189.84−37.24. Given the non-detection, we can restrict the mass of a compact cluster at this location to be less than $3.2 \times 10^{14}\ M_{\odot}$ at 68% confidence. However, the *Planck* data suggest that the source is quite large, in which case it is not surprising that nothing is seen in the CARMA data, which is insensitive to objects larger than ∼10′. Given its size, the object would have to be nearby, which makes it unlikely that it would have escaped detection in *ROSAT* if it is a genuine cluster. We conclude that the source is likely to be a dusty "cold-core" object associated with the Galactic plane.

The steep decline of the radio-source population with frequency makes the intrinsic contribution of contaminating sources to the 31 GHz CARMA data quite small (Muchovej et al. 2010); a total of three compact sources were removed from the observations of PLCKESZ G115.71+17.52 and PLCKESZ G121.11+57.01. The hybrid array configuration allows these sources to be cleanly removed from the short-baseline data with little impact on the final cluster parameters. In the case of PLCKESZ G189.84−37.24 there is no evidence for contaminating sources present in the data.

This work, combined with follow-up with *XMM-Newton* (Planck Collaboration et al. 2011c), a combination of AMI and *WISE* (Planck Collaboration et al. 2011a; AMI Consortium et al. 2011), and SPT observations of unconfirmed southern sources (Story et al. 2011), confirms all newly discovered clusters in the *Planck* ESZ catalog, with the exception of PLCKESZ G189.84−37.24. Under the assumption that this is not a genuine cluster, we conclude that the purity of the ESZ catalog is better than 99.5%.

We thank the staff of the Owens Valley Radio Observatory and CARMA for their outstanding support. We especially thank John Carlstrom for his efforts in spearheading the construction and operation of the SZA and for useful comments on the manuscript. Support for CARMA construction was derived from the Gordon and Betty Moore Foundation, the Kenneth T. and Eileen L. Norris Foundation, the James S. McDonnell Foundation, the Associates of the California Institute of Technology, the University of Chicago, the states of California, Illinois, and Maryland, and the National Science Foundation. Ongoing CARMA development and operations are supported by the National Science Foundation under a cooperative agreement (grant AST 08-38260) and by the CARMA partner universities (in particular NSF grant AST 0838187). S.M. gratefully acknowledges support from an NSF Astronomy and Astrophysics Fellowship.

Facilities: SZA, CARMA

REFERENCES

AMI Consortium, Hurley-Walker, N., Brown, M. L., Davies, M. L., et al. 2011, MNRAS, 414, L75
Arnaud, M., Pratt, G. W., Piffaretti, R., et al. 2010, A&A, 517, A92
Birkinshaw, M. 1999, Phys. Rep., 310, 97
Bonamente, M., Joy, M. K., Carlstrom, J. E., Reese, E. D., & LaRoque, S. J. 2004, ApJ, 614, 194
Bonamente, M., Joy, M. K., LaRoque, S. J., et al. 2006, ApJ, 647, 25
Bryan, G. L., & Norman, M. L. 1998, ApJ, 495, 80
Carlstrom, J. E., Holder, G. P., & Reese, E. D. 2002, ARA&A, 40, 643
Itoh, N., Kohyama, Y., & Nozawa, S. 1998, ApJ, 502, 7
Jones, M. E. 2002, in ASP Conf. Ser. 257, AMiBA 2001: High-Z Clusters, Missing Baryons, and CMB Polarization, ed. L.-W. Chen, C.-P. Ma, K.-W. Ng, & U.-L. Pen (San Francisco, CA: ASP), 35
Joy, M., LaRoque, S., Grego, L., et al. 2001, ApJ, 551, L1
LaRoque, S. J., Bonamente, M., Carlstrom, J. E., et al. 2006, ApJ, 652, 917
LaRoque, S. J., Joy, M., Carlstrom, J. E., et al. 2003, ApJ, 583, 559
Larson, D., Dunkley, J., Hinshaw, G., et al. 2011, ApJS, 192, 16
Marriage, T. A., Acquaviva, V., Ade, P. A. R., et al. 2011, ApJ, 737, 61
Melin, J.-B., Bartlett, J., Delabrouille, J., Piffaretti, R., & Pratt, G. W. 2011, A&A, 545, A139
Mohr, J. J., Mathiesen, B., & Evrard, A. E. 1999, ApJ, 517, 627
Mroczkowski, T., Bonamente, M., Carlstrom, J. E., et al. 2009, ApJ, 694, 1034
Muchovej, S., Leitch, E., Carlstrom, J. E., et al. 2010, ApJ, 716, 521
Muchovej, S., Leitch, E., Carlstrom, J. E., et al. 2011, ApJ, 732, 28
Muchovej, S., Mroczkowski, T., Carlstrom, J. E., et al. 2007, ApJ, 663, 708
Plagge, T., Benson, B. A., Ade, P. A. R., et al. 2010, ApJ, 716, 1118
Planck Collaboration, Ade, P. A. R., Aghanim, N., Arnaud, M., et al. 2011a, A&A, 536, A8
Planck Collaboration, Ade, P. A. R., Aghanim, N., Arnaud, M., et al. 2011b, A&A, 536, A23
Planck Collaboration, Aghanim, N., Arnaud, M., Ashdown, M., et al. 2011c, A&A, 536, A9
Planck Collaboration, Aghanim, N., Arnaud, M., Ashdown, M., et al. 2011d, A&A, 536, A10
Rudy, D. J. 1987, PhD thesis, California Institute of Technology, Pasadena
Story, K., Aird, K. A., Andersson, K., et al. 2011, ApJ, 735, L36
Sun, M., Sehgal, N., Voit, G. M., et al. 2011, ApJ, 727, L49
Sunyaev, R. A., & Zel'dovich, Y. B. 1970, Comments Astrophys. Space Phys., 2, 66
Sunyaev, R. A., & Zel'dovich, Y. B. 1972, Comments Astrophys. Space Phys., 4, 173
Vanderlinde, K., Crawford, T. M., de Haan, T., et al. 2010, ApJ, 722, 1180
Weiland, J. L., Odegard, N., Hill, R. S., et al. 2011, ApJS, 192, 19
Wen, Z. L., Han, J. L., & Liu, F. S. 2009, ApJS, 183, 197